

PAPER • OPEN ACCESS

Instabilities in electrically driven rotating MHD layers

To cite this article: C Mistrangelo and L Bühler 2017 *IOP Conf. Ser.: Mater. Sci. Eng.* **228** 012004

View the [article online](#) for updates and enhancements.

Related content

- [Numerical comparisons of the performance of a hydraulic coupling with different pump rotational speeds](#)
Y Luo, L H Feng, S H Liu et al.
- [Origin of Hysteresis-like Behavior in Flow Transition in Simulations of the Czochralski Method with Tetradecane](#)
Hiroshi Kimura
- [Three-dimensional MHD flow over a shrinking sheet: Analytical solution and stability analysis](#)
Sumaira Afzal, Saleem Asghar and Adeel Ahmad

Instabilities in electrically driven rotating MHD layers

C Mistrangelo and L Bühler

Karlsruhe Institute of Technology, P.O.B. 3640, 76021 Karlsruhe, Germany

chiara.mistrangelo@kit.edu

Abstract. Flows of electrically conducting fluids exposed to intense magnetic fields exhibit a common feature i.e. the formation of uniform cores in which electromagnetic forces are dominant. Cores are separated from each other by thin layers that extend along magnetic field lines. Across these parallel layers strong gradients of flow variables are present, which can lead to the onset of instabilities and non-linear flow transitions.

In this work we investigate dynamics and stability issues of rotating parallel layers driven by electromagnetic forces caused by the interaction of injected electric currents with an applied magnetic field. The geometry considered consists of two coaxial circular electrodes used for current injection. They are placed in parallel electrically insulating planes perpendicular to a uniform magnetic field. The basic axisymmetric steady state flow, characterized by a rotating velocity jet confined in a parallel layer that connects the rims of the electrodes, is rather well understood. By increasing the driving current above a critical value the basic flow becomes unstable and undergoes a sequence of supercritical bifurcations.

1. Introduction

Electrically driven magnetohydrodynamic (MHD) flows have been investigated numerically for the experimental configuration used in [1] and a test-section has been manufactured and instrumented to study MHD phenomena observed in the simulations. Electric current is injected between two coaxial, parallel circular electrodes, which are perpendicular to an externally applied uniform magnetic field. As a result of the MHD interaction of current and magnetic field, an azimuthal flow originates that is mainly confined in an annular fluid layer, which connects the rims of the electrodes. A similar type of flow can appear also in large scale phenomena typical of geo- and astrophysics [2]. The aim of the present study is getting an overview of unstable flow patterns that occur when the current injected across the liquid metal layer is increased above a critical value [3] [4].

In the past experiments and analytical studies have been carried out to investigate MHD flows, where the fluid is set in motion by electromagnetic forces generated by current injected between a pair of concentric electrodes on the bottom of an electrically insulating container [5] [6] [7]. These studies can be regarded as the electrical analogon of those performed in [8]. The established flow consists of a rotating annular core and two shear layers, aligned with the magnetic field. Here the current flows in axial direction before closing through the Hartmann layers that form along surfaces perpendicular to the magnetic field. The width δ of the internal layers reduces by increasing the magnetic field strength as $\delta \sim Ha^{-1/2}$. The Hartmann number Ha gives a non-dimensional measure for the strength of the imposed magnetic field. This flow distribution differs from the one described in this work, where cores are stagnant and the induced stationary rotating motion consists of jets confined in an internal parallel layer. Here the maximum jet-velocity increases with Ha and the flow in the layer can become unstable.



MHD flows created by injecting current through circular electrodes of finite diameter, as considered in the present study, are discussed in [1]. An approximate steady state asymptotic solution is developed and compared with experiments. For high Hartmann numbers the current is confined to the cylinder of fluid between the electrodes and when reducing the magnetic field the electric resistance of the fluid decreases due to the spread of current streamlines across the enlarged internal layer. The established azimuthal velocity distribution results from the balance between viscous and electromagnetic Lorentz forces in the layer. Discrepancies between experiments and asymptotic solution are explained by suggesting the occurrence of an axial-radial secondary flow. The contribution of the latter is not taken into account in [1]. A more rigorous asymptotic solution for the description of a steady, electrically driven shear layer is given in [9]. Experiments in [1] were carried out in a range of parameter where the flow is expected to be stable. Local electric potential was measured by using a potential probe and velocities by a Pitot tube. An attempt to investigate experimentally instabilities that occur in this type of electrically driven flows can be found in [10] [11], where instantaneous velocities are measured by means of hot-film anemometry. Experiments were reproducible only for sufficiently intense magnetic fields and data could be obtained for a limited range of parameters, $300 < Ha < 650$. Considerable deviations between experiments and theoretical studies [9] were observed and explained by a deterioration of measurements due to the influence of magnetic field on heat transfer properties of the hot-film sensor and the occurrence of contributions from the radial velocity. Malcolm [11] finds that for large magnetic fields the critical current for the onset of instabilities and the corresponding Reynolds number vary as $I_c \sim Ha^{4/3}$ and $Re_c \sim Ha^{1/3}$, respectively. Empirical observations point out that instability sets in as wave-like flow with steady amplitude.

Available theoretical studies of electrically driven MHD flows neglect the contribution of radial and axial velocities. In our analysis we consider this additional superimposed secondary circulation, the magnitude of which can be used to estimate the degree of anisotropy of the established MHD flow. For the described MHD flows only very few experimental results are available. Hence an experimental program has been proposed to thoroughly investigate instabilities in electrically driven rotating layers.

2. Formulation of the problem

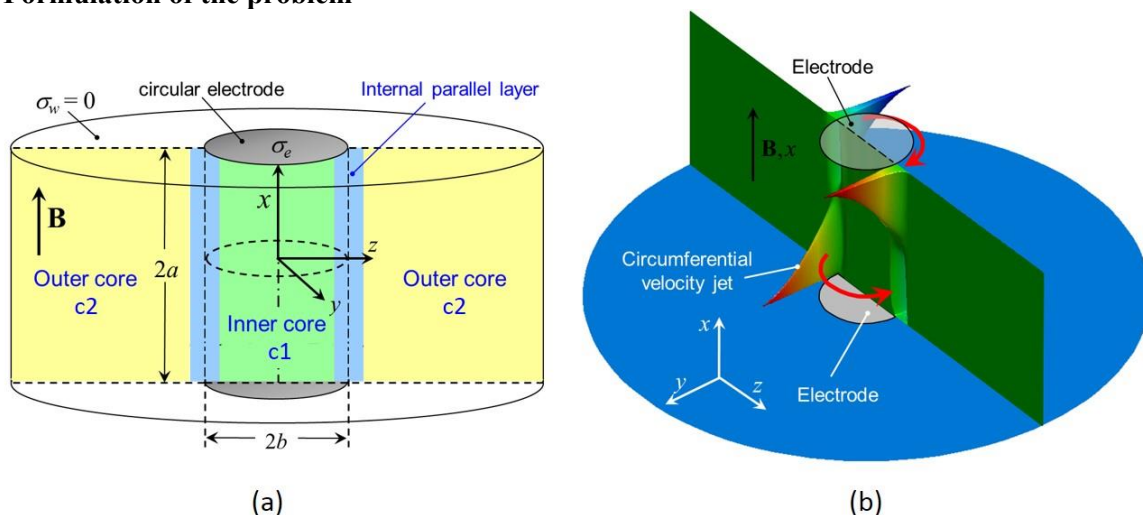


Figure 1. (a) Sketch of the geometry used for the simulations and main typical flow regions: an internal layer separates an inner and an outer core (c1 and c2). (b) Velocity distribution in case of a stable, laminar flow.

The geometry considered is schematically depicted in Figure 1a. We investigate the liquid metal flow in an electrically insulating cylindrical container of height $2a$ with two perfectly conducting electrodes

embedded in the top and bottom walls, when a uniform magnetic field $B\hat{\mathbf{x}}$ is applied aligned with the axis of the container. The electrodes are kept at constant electric potential so that a potential difference $\Delta\phi$ is present between them. Half of the distance a between the electrodes has been chosen as characteristic size of the problem. The electrode rim is located at $b/a = 0.5$, where b is the electrode radius. The imposed potential difference $\Delta\phi$ drives a current between the electrodes and the resulting electromagnetic forces induce a primary azimuthal flow that is practically located inside a thin parallel layer originating from the electrode rims. The shear layer is caused by the discontinuity in the electrical boundary conditions on the top and bottom of the cylinder.

If $\Delta\phi$ is smaller than a critical value a steady state solution establishes and the layer takes the shape of a velocity jet travelling in circumferential direction. The 3D velocity distribution for a stable MHD flow is depicted in Figure 1b.

The established MHD flow can be mathematically described by equations for conservation of momentum, mass and charge that in non-dimensional form can be written as

$$\frac{1}{N} \left[\frac{\partial \mathbf{v}}{\partial t} + (\mathbf{v} \cdot \nabla) \mathbf{v} \right] = -\nabla p + \frac{1}{Ha^2} \nabla^2 \mathbf{v} + \mathbf{j} \times \mathbf{B}, \quad (1)$$

$$\nabla \cdot \mathbf{v} = 0, \quad \nabla \cdot \mathbf{j} = 0, \quad (2)$$

where the current density \mathbf{j} is expressed by Ohm's law

$$\mathbf{j} = -\nabla\phi + \mathbf{v} \times \mathbf{B}. \quad (3)$$

The variables \mathbf{v} , p , \mathbf{j} , \mathbf{B} and ϕ indicate velocity, pressure, current density, magnetic field and electric potential normalized by u_0 , $\sigma u_0 B^2 a$, $\sigma u_0 B$, B , and $u_0 B a$, respectively. Here B is the magnitude of the magnetic field, and u_0 a typical velocity. The electrical conductivity σ , the density ρ and the kinematic viscosity ν of the fluid remain constant. It is assumed that the magnetic field induced by the flow is negligible compared to the imposed field. This assumption is called inductionless approximation and it is valid for small magnetic Reynolds numbers, $R_m = \mu \sigma a u_0 \ll 1$, where μ is the magnetic permeability [12].

The dimensionless groups in (1) are the interaction parameter N and the Hartmann number Ha :

$$N = \frac{\sigma a B^2}{\rho u_0}, \quad Ha = a B \sqrt{\frac{\sigma}{\rho \nu}}. \quad (4)$$

The former one describes the ratio between electromagnetic and inertia forces, the latter gives a non-dimensional measure for the strength of the magnetic field. Its square quantifies the ratio of electromagnetic to viscous forces. The magnitude of the potential difference $\Delta\phi$ between the electrodes is expressed in dimensionless form by the Reynolds number Re

$$Re = \frac{\Delta\phi}{2} \frac{1}{B \nu}. \quad (5)$$

As electric boundary conditions fixed potential values are set at the electrodes, while the external surface of the cylinder is electrically insulated, i.e. $\partial_n \phi = 0$. The no slip condition, $\mathbf{v} = 0$, is applied to all walls.

3. Numerical results

Data from numerical simulations are discussed for a constant Hartmann number, $Ha = 588$, and various Reynolds numbers. The selected Hartmann number has been chosen since for this magnetic field strength experimental and theoretical data for stationary conditions are available in literature [9].

The code used for the numerical simulations has been obtained by introducing the Lorentz force term and the equations determining electric current density and potential into the finite volume open source code OpenFOAM.

3.1. Steady solution

For $\Delta\phi < 140\mu\text{V}$ ($Re < 500$) a steady state solution is found, which is characterized by two counter rotating layers (see Figure 1b) mainly confined in an annular region that separates an internal and an external core as schematically displayed in Figure 1a. The fluid is stagnant both in the internal and in the external cores and it moves with a jet-like profile inside the parallel layer. The 3D velocity distribution for a stable laminar MHD flow at $Ha = 588$ and $Re = 358$ is depicted in Figure 1b.

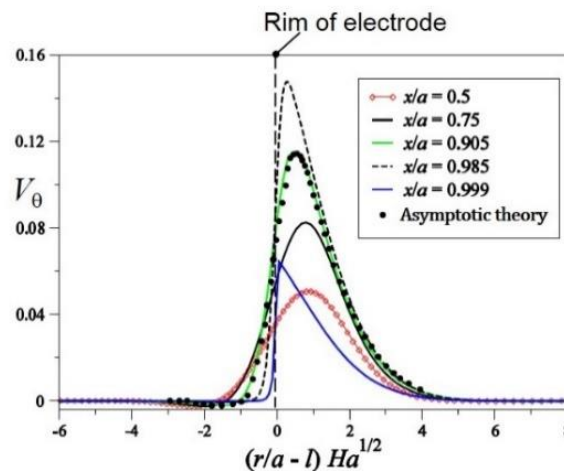


Figure 2. Radial profile of scaled azimuthal velocity for a steady flow at $Ha = 588$, at different axial locations. The velocity profile at $x/a = 0.905$ agrees well with the available asymptotic solution [9].

In Figure 2 the scaled circumferential velocity $V_\theta = v_\theta Ha^{1/2} bl(\sigma\rho\nu)^{1/2}/I$ is plotted along the normalized radial direction at various axial positions x/a for a stable MHD flow at $Ha = 588$. The total driving current density is named I . The velocity is scaled according to [9]. The predicted velocity profile at $x/a = 0.905$ reproduces well the one from the asymptotic solution indicated by dots, as given in [9]. This suggests that, for the potential difference considered, inertia effects are negligible compared to electromagnetic and viscous forces, and the secondary flow in axial direction is much weaker than the circumferential flow, as assumed in the cited theoretical study. The magnitude of the circumferential velocity increases linearly from zero at the symmetry plane to a maximum value when approaching the Hartmann walls perpendicular to \mathbf{B} . In the Hartmann layers the velocity reduces with a strong gradient over a distance of $O(Ha^{-1})$ to satisfy the no slip condition at the wall.

The layer takes the shape of a velocity jet travelling in circumferential direction, whose thickness δ remains constants when it rotates, as visualized in Figure 3. Here the potential ϕ and the axial vorticity component ω_x are plotted on a plane perpendicular to the magnetic field, at an axial coordinate $x/a = 0.5$, at half distance between electrode and symmetry plane. Across the internal layer, in radial direction, the electric potential drops from the inner core value ϕ_{c1} , which varies linearly along x , to $\phi_{c2} = 0$ in the outer core. The strong radial potential gradient primarily balances the induced electric field, and the potential difference $\phi_{c1} - \phi_{c2}$ through the layer is responsible for the formation of the rotating jet. The vorticity profile along the dashed line in the middle of the geometry at $z = 0$ (see Figure 3b) exhibits maxima and minima as marked by green stars. The occurrence of instabilities of the flow in the layers is associated with the presence of extrema in the vorticity field that correspond to inflection points in the velocity profile.

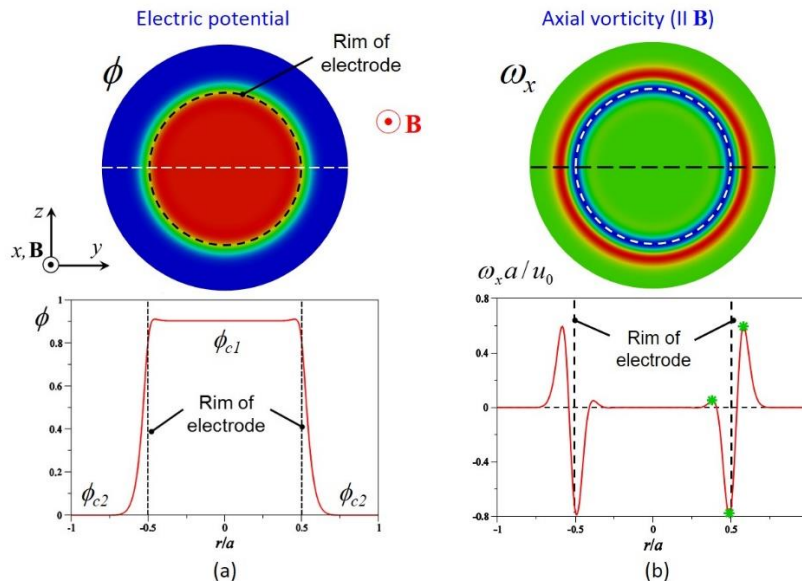


Figure 3. Results for a steady state flow at $Ha = 588$. (a) Electric potential distribution and (b) contours of axial vorticity on a plane at $x/a = 0.5$. Potential and vorticity are also plotted along the dashed line in the middle of the geometry.

3.2. Unstable flow regime

Simulations have been performed by increasing the applied potential difference, i.e. the Reynolds number, while holding the magnetic field constant, $Ha = 588$.

In Figure 4a the normalized time-averaged circumferential velocity is plotted along the scaled radial direction at $x/a = 0.905$ for various Reynolds numbers. By increasing Re the maximum of the azimuthal velocity reduces and shifts to higher radial positions. The negative velocity at the interface between inner core and layer progressively disappears, and a minimum occurs in the outer core. The time-averaged thickness δ of the internal layer becomes larger and the mean velocity in the jet reduces due to the increased transfer of momentum related to the occurrence of time-dependent fluctuations. This behavior is analogous to the one of unstable MHD flows in field-aligned boundary layers in ducts, although the physics behind the phenomena is different [13] [14] [15].

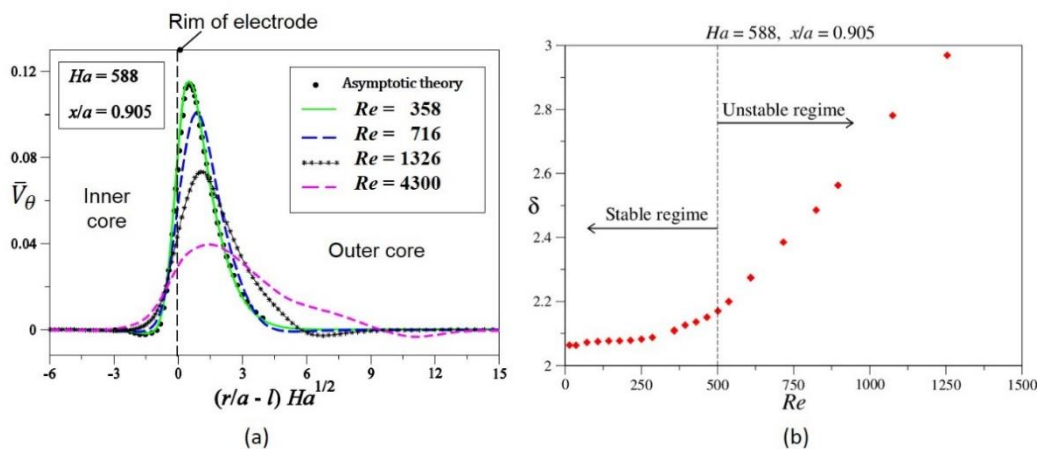


Figure 4. Flow at $Ha = 588$ and various Reynolds numbers. (a) Radial profile of scaled time-averaged azimuthal velocity at the axial location $x/a = 0.905$, for various applied potential differences (Re). (b) Thickness δ of the internal layer as a function of the Reynolds number.

In Figure 4b the thickness δ of the internal layer, estimated as the ratio between the integral of the velocity profile V_θ and its maximum $V_{\theta\max}$, is plotted as a function of the Reynolds number. For $100\mu\text{V} < \Delta\phi < 140\mu\text{V}$, i.e. $350 < Re < 500$, the flow is still steady and one could expect that δ remains constant. However, the internal layer thickens and flow structures extend to larger radial positions due to the occurrence of an increasing radial velocity. In the inertialess limit ($Re \rightarrow 0$) the thickness of the internal layers parallel to the magnetic field should scale as $Ha^{-1/2}$. In the present problem, when secondary flow and time dependent flow structures appear, the thickness δ of the layer can depend on the interaction parameter N , or a combination of N and Ha . This is due to the fact that radial-axial flow and unstable patterns are caused by inertial forces.

For $Re > 500$ the flow becomes unstable in agreement with experiments in [11]. The instability sets in as sinusoidal oscillations and vortices develop, which have a main vorticity component ω_x in magnetic field direction.

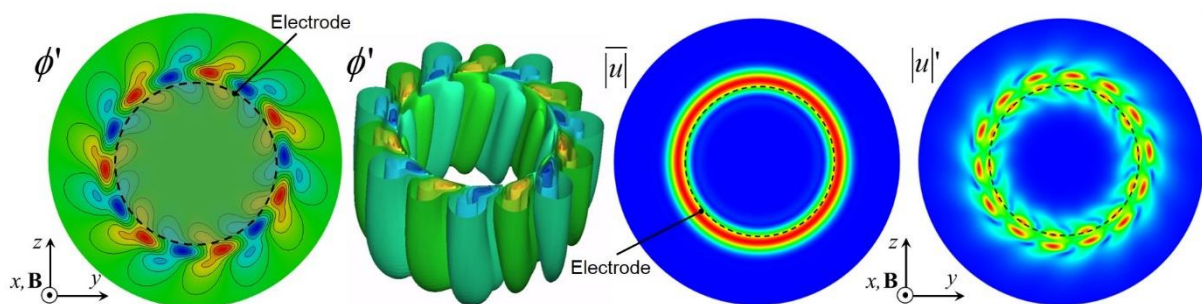


Figure 5. Example of unstable flow at $Ha = 588$ and $Re = 540$. Plots show contours of fluctuating part ϕ' of electric potential, magnitude of the mean velocity, fluctuations of the velocity magnitude, on a plane perpendicular to \mathbf{B} at $x/a = 0.5$.

An example of unstable flow is visualized in Figure 5 for $Re = 540$. Here contours of the fluctuating part $\phi' = \phi - \bar{\phi}$ of electric potential, mean part and fluctuations of the magnitude of the velocity are plotted on a plane perpendicular to \mathbf{B} , at $x/a = 0.5$. The unstable regime is characterized by a periodic vortex pattern and the instability takes the form of a chain of small vortices. The amplitude of the fluctuations decreases when moving from the Hartmann walls to the symmetry plane where they vanish. The 3D view of the fluctuations ϕ' of the electric potential in Figure 5 clearly highlights the three-dimensionality of the unstable structures. Perturbations are conveyed by the mean flow, $|\mathbf{u}| = |\bar{\mathbf{u}}| + |\mathbf{u}'|$. Contours of axial vorticity are depicted in Figure 6 left.

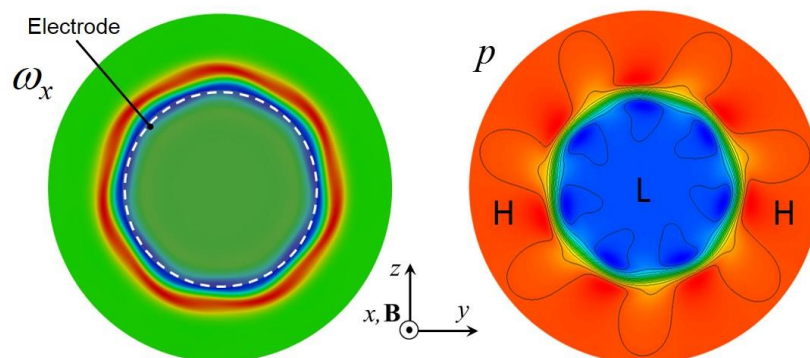


Figure 6. Contours of pressure p and axial vorticity ω_x on a plane perpendicular to \mathbf{B} at $x/a = 0.5$ for the unstable flow at $Ha = 588$ and $Re = 540$.

An interesting flow feature that did not receive adequate attention in the past is the occurrence of a radial-axial flow superposed to the main azimuthal circulation. The occurrence of this secondary flow was already suggested in [1] as an explanation for discrepancies between experiments and asymptotic solution, but an exhaustive description of the phenomenon was not given. Preliminary numerical calculations [3] show that the secondary flow consists of a motion towards the electrodes in the internal part of the layer and towards the symmetry plane in the external portion. This results in a centripetal flow near the symmetry plane and a centrifugal flow at the interface between core and Hartmann layer. This secondary motion is caused by a balance of pressure, electromagnetic and inertial centrifugal forces. The pressure force points towards the inner core as visible in Figure 6 on the right, where pressure contours are depicted on a plane perpendicular to \mathbf{B} at $x/a = 0.5$. The electromagnetic Lorentz force slows down the secondary flow and balances the viscous forces in layers.

4. Experimental set up

The conceptual design of the fabricated test-section is shown in Figure 7a. It consists of a vessel filled with the eutectic alloy GaInSn. On the electrically insulating top and bottom walls that are perpendicular to the imposed magnetic field (Hartmann walls) two circular coaxial copper electrodes with radius b are inserted flush with the internal surface of the plates. The axial length of the electrodes has been selected long enough to achieve sufficiently homogeneous current density at the fluid-solid interface. According to the numerical results, the diameter D of the outer cylinder has been defined such that the lateral wall does not interact with the layer or with unstable vortex patterns. Another constraint for the size of the vessel is represented by the dimension of the bore of the superconducting magnet at TUI (376 mm), where experiments will be performed. A reasonable choice is $D = 9b$.

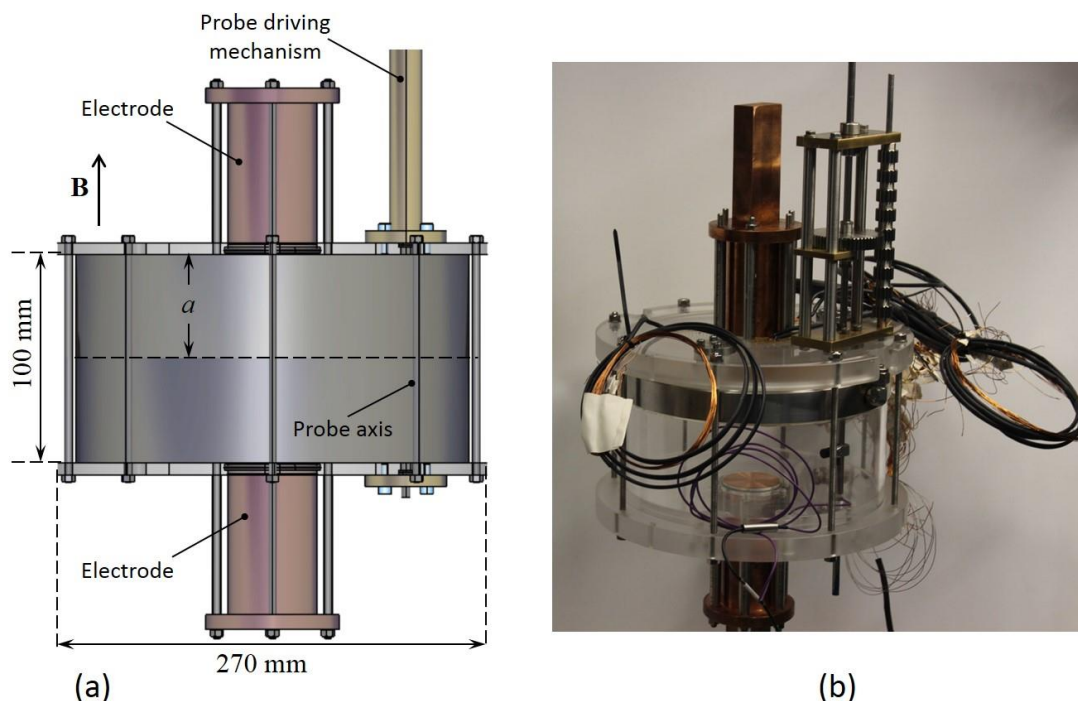


Figure 7. (a) Design and (b) picture of the manufactured and fully instrumented test-section

The test-section is designed according to a modular design by using flanges to connect different components. This permits an easy replacement of the cylindrical container in order to investigate the

influence of the axial distance between the electrodes on onset and development of instabilities in the rotating fluid layer. This design flexibility allows also modifying the set-up of the instrumentation.

In order to preclude flow artifacts arising from symmetry deviations of the experimental configuration special care is required to ensure a precise positioning inside the magnet. The fluid vessel has to be placed concentrically inside the bore of the magnetic system.

4.1. Instrumentation

During the experimental campaign, values of local electric potential and potential differences are recorded by means of sensors located on Hartmann walls and by movable probes in the liquid metal. These data can be directly compared with numerical results. Spatial-temporal information about velocity field can be obtained by using ultrasound Doppler velocimetry (UDV) techniques. Temperature has also to be monitored at different locations on the test-section in order to calculate the physical properties of the liquid metal and to verify that experiments are carried out under isothermal operating conditions so that thermo-electric effects can be neglected. Figure 7b shows a picture of the fully instrumented test section and in Figure 8 the position of the various instruments is displayed.

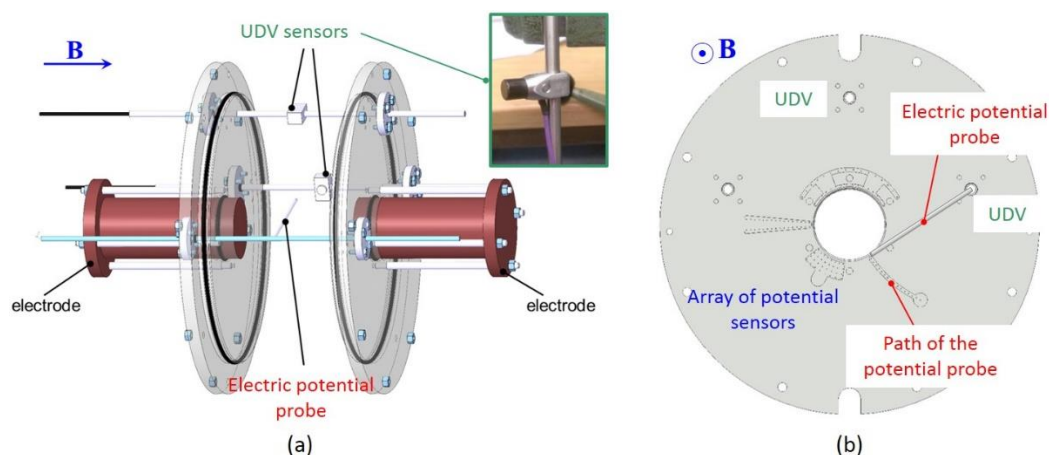


Figure 8. (a) Design of the test-section and available instrumentation: electric potential probe (red), UDV sensor (green). (b) Arrangement of electric potential sensors on the Hartmann wall of the container. The pins aligned along the path described by the movable probe are used to determine cross-correlation functions of potential fluctuations along magnetic field lines.

4.1.1. Electric potential probe

In order to determine local velocities in liquid metal flows electric potential differences, induced by the motion of an electrically conducting fluid in the imposed magnetic field, are measured by means of potential probes. Their operating principle is based on Ohm's law (3), through which the velocity components perpendicular to $\mathbf{B} = \hat{\mathbf{x}}$ can be expressed in non-dimensional form as

$$\mathbf{v}_{\perp} = \left(-\frac{\partial\phi}{\partial z} - j_z \right) \hat{\mathbf{y}} + \left(\frac{\partial\phi}{\partial y} + j_y \right) \hat{\mathbf{z}} \quad (6)$$

The local velocity is determined by potential gradients and by currents induced in the fluid. Therefore, the potential difference measured at the sensor tips can be directly interpreted in terms of velocity components only if the current density is very small or known [16].

In the planned experiments it is foreseen to employ a movable potential probe with four sensing tips in order to measure the intensity of time-dependent fluctuations of potential and potential gradients. A principle sketch of the probe is shown in Figure 9(a). Tips a and b are located on the same plane zy perpendicular to the magnetic field ($x_a = x_b$), while the central electrodes c are shifted along y and x with respect to tips a and b in order to measure fluctuations of the radial velocity. The body of

the movable electric potential probe consists of a carbon rod the diameter of which should be minimized in order to reduce the obstruction of the flow by the sensor (Figure 9(b)). Due to circumferential symmetry of the flow it is not possible to record average profiles of radial velocity, since the mean potential is constant along a circumference. However, fluctuations of the radial velocity can be measured. Detection of the onset of these oscillations, compatibly with the accuracy of measuring instruments, could be an efficient method to identify the stability limit as a function of Reynolds and Hartmann numbers. Measurements of fluctuations of the much larger circumferential velocity require the average value to be filtered out before amplifying it.

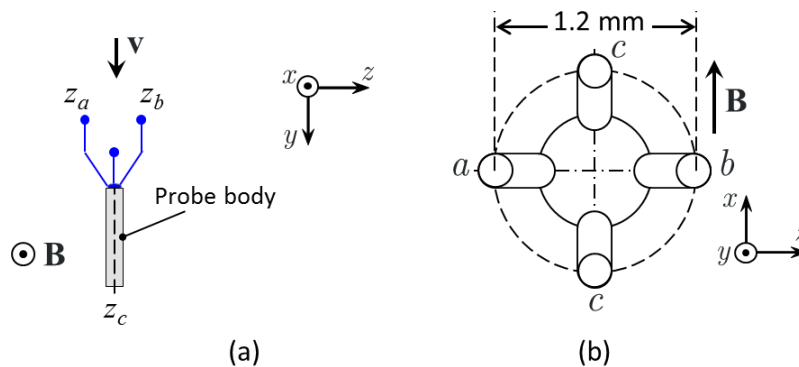


Figure 9. (a) Sketch of an electric potential probe to record local potential values and gradients. The probe has four sensing tips. (b) Frontal view of the probe.

4.1.2. Electric potential sensors on Hartmann wall

The distribution of potential gradient on walls perpendicular to the applied magnetic field can be directly related to the flow velocity. It gives information about flow structure at the interface between Hartmann layer and core of the flow if two conditions are satisfied. First there should be no variation of the electric potential across the thin Hartmann layer, i.e. the potential at the wall coincides with the value at the core-layer interface, and second the current density at the core-layer edge is negligible. Under these assumptions measurements of electric potential on the Hartmann walls allow obtaining an estimate of velocity components on a plane orthogonal to the magnetic field. Comparison with numerical simulations can support the proper physical interpretation of recorded quantities.

In order to measure the two dimensional distribution of the electric potential on a plane perpendicular to the magnetic field, an array of sensors (copper pins) has been installed on the Hartmann wall as shown in Figure 8b. They are in electrical contact with the liquid metal. This array permits to reconstruct an image of vortex patterns, i.e. to map the electric potential distribution at the core-Hartmann layer interface. The sensors are located along radii and regularly spaced along concentric circles. The spacing between the pins is selected so that higher spatial resolution is guaranteed. The proper distance is chosen according to numerical results that allow identifying small scale recirculating flow patterns. Signal correlations between points on the same circumference allow determining the travelling speed of the waves, the wave number and therefore the number of vortices forming the fluctuating patterns.

Electric potential sensors on the Hartmann wall are also located along a circle that corresponds to the path of the movable probe (see Figure 8b). In this way it is possible to define correlations between pairs of measured electric potential fluctuations recorded simultaneously at corresponding points along the same magnetic field line.

5. Conclusions and future work

Numerical simulations have been performed to study the stability of rotating liquid metal layers that are driven by MHD interaction of injected currents with an imposed magnetic field. Two coaxial electrodes are inserted in insulating parallel plates, which are perpendicular to an imposed magnetic

field. The basic steady state flow consists of two counter rotating layers whose velocity vanishes at the symmetry plane. The maximum velocity is reached near the Hartmann layers. The radial profile of the azimuthal velocity exhibits inflection points and for sufficiently large driving current, the flow becomes unstable.

At the onset of instability the flow pattern is characterized by a chain of periodic small vortices. By increasing the Reynolds number the vortices merge together to give rise to larger structures.

An experimental test-section has been fabricated and it will be inserted in the superconducting magnet at the technical university of Ilmenau (TUI). The aim is both complementing the numerical results and comparing the measured data with the simulations. A stability map will be defined to identify the different flow regimes depending on Reynolds and Hartmann numbers.

During the experiments electric potential will be recorded on the Hartmann walls of the cylinder as well as inside the liquid metal by means of a movable probe.

Acknowledgement

Financial support of this research by the German Helmholtz Association in the frame of the Helmholtz-Alliance LIMTECH is gratefully acknowledged.

References

- [1] J. C. R. Hunt and D. G. Malcolm 1968 *Journal of Fluid Mechanics* **33** 775
- [2] R. Hollerbach 2000, in *Physics of Rotating Fluids*, vol. 549, C. Egbers and G. Pfister, Eds., Springer, pp. 295-316
- [3] C. Mistrangelo and L. Bühler 2011, in *Proceedings of the 8th Pamir International Conference on Fundamental and Applied MHD, Borgo, Corsica September 5-9*, pp. 175-179
- [4] C. Mistrangelo and L. Bühler 2015, in *6th International Symposium on Bifurcations and Instabilities In Fluid Dynamics, Paris, July 15-17*
- [5] V. B. Levin 1980 *Magnetohydrodynamics* **16** 70
- [6] A. A. Klyukin, Y. B. Kolesnikov and V. B. Levin 1980 *Magnetohydrodynamics* **16** 75
- [7] A. A. Klyukin and V. B. Levin 1984 *Fluid Dynamics* **19** 815
- [8] B. Lehnert 1955 *Proceedings of The Royal Society London A* **233** 299
- [9] J. C. R. Hunt and K. Stewartson 1969 *Journal of Fluid Mechanics* **38** 225
- [10] D. G. Malcolm 1969 *Nature* **224** 909
- [11] D. G. Malcolm 1970 *Journal of Fluid Mechanics* **41** 531
- [12] P. H. Roberts, The Whitefriars Press Ltd., London and Tonbridge, 1967.
- [13] U. Burr, L. Barleon, U. Müller and A. B. Tsinober 2000 *Journal of Fluid Mechanics* **406** 247
- [14] L. Bühler and S. Horanyi 2009 *Fusion Engineering and Design* **84** 518
- [15] M. Kinet, B. Knaepen and S. Molokov 2009 *Physical Review Letters* **103**, 154501
- [16] A. Kolin and F. Reiche 1954 *Journal of Applied Physics* **25** 409